Earth and Space Science

RESEARCH ARTICLE
10.1029/2018EA000377

Special Section:
Science and Exploration of the Moon, Near-Earth Asteroids, and the Moons of Mars

Variability of Spatter Morphology in Pyroclastic Deposits in Southern Idaho, as Correlated to Thermal Conditions and Eruptive Environment

E. Rader[1,2], S. Kobs Nawotniak[3], and J. Heldmann[1]

[1]NASA Ames Research Center, Moffett Field, CA, USA, [2]University of Idaho, Moscow, ID, USA, [3]Idaho State University, Pocatello, ID, USA

Key Points:
- Study catalogs pyroclast size and morphology on a variety of spatter features
- Thermal conditions of deposition are reflected in the fusion between clasts as well as the degree of elongation of the clasts
- Spatter erupted in cooler environments (secondary spatter) may show different clast morphology (size, shape, and amount of fusion between clasts) than primary vent spatter

Supporting Information:
- Supporting Information S1
- Table S1
- Table S2
- Table S3
- Table S4

Correspondence to:
E. Rader,
erika.rader@nasa.gov

Citation:
Rader, E., Kobs Nawotniak, S., & Heldmann, J. (2018). Variability of spatter morphology in pyroclastic deposits in Southern Idaho, as correlated to thermal conditions and eruptive environment. *Earth and Space Science*, *5*, 592–603. https://doi.org/10.1029/2018EA000377

Received 14 FEB 2018
Accepted 19 SEP 2018
Accepted article online 28 SEP 2018
Published online 13 OCT 2018

Abstract To investigate the thermal conditions of spatter eruptions on Earth, other planets, and moons we measured and categorized the physical characteristics of clasts in spatter deposits in Southern Idaho, USA. Physical characteristics of clasts, such as aspect ratio and degree of welding, are influenced by the style of eruption, distance from the vent, and lava properties. The correlation between morphological characteristics and the degree of fusion constrains thermal conditions of unwitnessed spatter-producing eruptions on Earth and extraterrestrial volcanoes. We categorize spatter deposits into three groups, as defined by their emplacement conditions: primary vent, distal (spatter exposed in noneruptive cracks on the flanks of primary vents), and hornito (secondary spatter from a nonprimary cone); and show the variability of clast morphology within the three categories. Primary vent deposits typically show a wide range of fused perimeters between clasts (18–82%), lower aspect ratios (0.20–0.49), and larger void space, both between clasts (4–21%) and within clasts (referred to as hollow cores, up to 93%). Hornitos typically have less fusion (14–22%) between clasts, higher aspect ratios (0.45–0.49), and lower proportions of void space (6–10%). Distal outcrops are easily distinguished by the lack of void space (<8%) and the very high aspect ratio of clasts (close to 1). When chemical composition and outcrop proximity are accounted for, the accumulation rate appears to be primarily responsible for spatter clast morphology. Our results are based on field measurements of clasts; however, digital imagery could be used to categorize and interpret pyroclastic deposits in planetary systems by robotic spacecraft.

Plain Language Summary The way spatter deposits look (clash shape, size, etc.) changes with temperature. Hotter deposits from close to the vent can be distinguished from cooler deposits emplaced far from the heat source. This may have implications for using volcanic deposits to detect different eruption environments.

1. Introduction

Spatter deposits only form in a narrow range of eruptive conditions including deposition temperature, accumulation rate, and eruption explosivity (Head & Wilson, 1989; Sumner, 1998; Sumner et al., 2005; Rader & Geist, 2015). The rheology of clasts during and immediately after flight is sensitive to these same conditions, resulting in clast morphologies that are reflective of the thermal conditions of emplacement. Different thermal conditions may result from lava interacting with water, or because the eruption was waxing and waning (e.g., Mattox & Mangan, 1997; Sumner, 1998). For unwitnessed eruptions, differences in spatter clast morphology may provide a method to distinguish between water interaction (which can result in rootless cones) or varying eruption intensity. Rootless cones are often composed of alternating layers of cinder and spatter with a thicker cap of spatter agglutinate on the top (Fagents & Thordarson, 2007; Hamilton et al., 2010, 2017; Jurado-Chichay et al., 1996; Reynolds et al., 2016; Thordarson et al., 1992; Thordarson & Hoskuldsson, 2002). While the primary material in rootless cones is scoria, the already hardened scoria clasts do not record the thermal conditions of a deposit as well as spatter clasts (Rader & Geist, 2015).

Spatter deposits (Figure 1) comprised of once fluid fragments of lava that were ejected out of a partially molten lava pond. The accumulation of these fragments (clasts) results in deposits that have steep sides as well as lumpy surface texture, irregular distribution of void spaces within the outcrop, and variable coloration (e.g., white, yellow, orange, maroon) due to different degrees of primary oxidation or alteration to the typically black lava that occurred during or shortly after eruption. Deposits that form along a linear vent are typically called *spatter ramparts*, whereas conical shapes are referred to as *spatter cones*. Upon ejection,

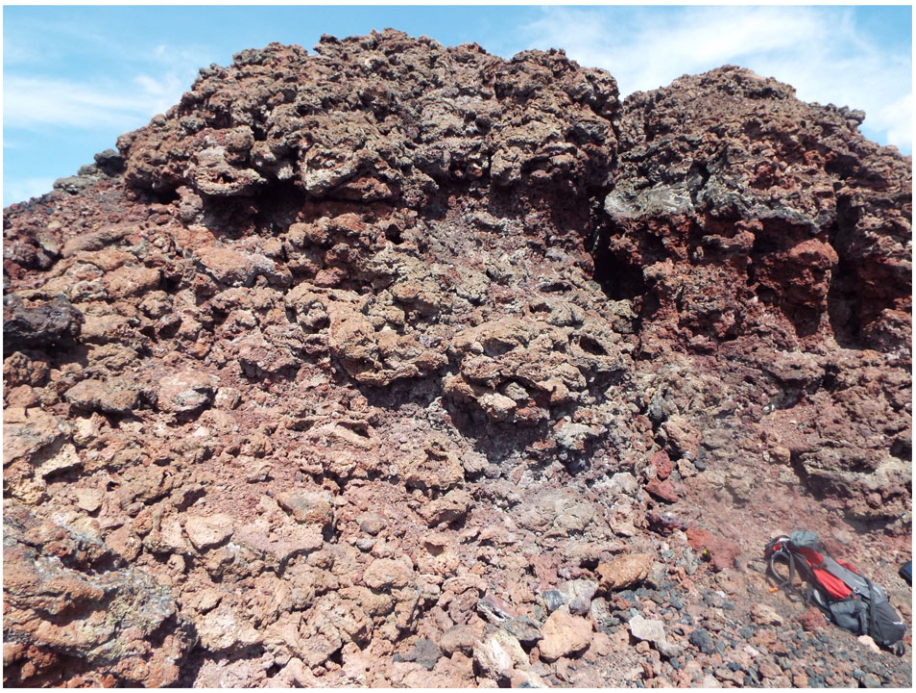

Figure 1. A photograph of the outer wall of a spatter deposit exhibiting a typical *lumpy* morphology. This deposit (COTM16-01) also has extensive red oxidation of the iron contained in the glassy rims of the clasts. Note the backpack for scale.

clasts develop a semiflexible skin as the exterior quenches. The interior will remain hot for longer. Due to the different cooling rates, different vesicle and crystal textures develop in the outer and inner portions of the clast (e.g., Jones et al., 2018; Shin et al., 2005; Sumner et al., 2005, Stovall et al., 2012). The rate of heat loss in a spatter pile is affected by the initial temperature and size of the clasts, the duration of flight, and the thermal environment of deposition such as accumulation rate, proximity to the vent, and presence of meteoric water (Capaccioni & Cuccoli, 2005; Head & Wilson, 1986; Rader & Geist, 2015; Sumner et al., 2005). An increase in thermal flux from faster accumulation rates or higher temperatures results in greater fusion between clasts in laboratory simulations of spatter clasts (Rader & Geist, 2015). Clasts that are smaller, are airborne longer, are deposited slowly or far from the vent, or interact with a hydrous environment will all cool faster, resulting in a poorly fused deposit. Untangling the effect of initial, eruptive, and depositional conditions may allow for spatter deposit interpretation on Earth and Mars using clast measurements such as vesicularity, quench rind thickness, or clast size and shape.

Eruptive environments of spatter include primary vents, where magma reaches the surface. The presence of spatter at these sorts of features has been used in studies of ancient deposits to signal eruption location and eruption vigor (e.g., Brown et al., 2014). Sufficiently large eruptions may produce cones or ramparts that, later bisected by cracks, expose distally located spatter clasts that were launched meters to tens of meters from the vent center. Other eruptive environments of spatter have been deemed *rootless* or *secondary* features (e.g., Bruno et al., 2006; Fagents & Thordarson, 2007; Jones et al., 2018; Reynolds et al., 2015), a designation typically used to indicate the interaction of lava with surface or near-surface water. Hornitos (Figure 2) are a type of secondary cone, which can form from the interaction of water (Gao et al., 2010), or from the buildup of pressurized gas in a very full lava tube (Kauahikaua et al., 2003). The greater distance from the primary vent gives lava time to cool and degas before producing clasts at the hornito. While hornitos are essentially cones without a root (a connection to a magma source), the term *rootless cone* is so frequently associated with water interaction that we will only use hornito in this paper to refer to the secondary spatter features formed when no water was present.

Typically, spatter outcrops in the field are assumed to be a primary vent feature, especially if the deposit is linear, if voluminous flows originate from the area, and no evidence of water is present (such as a

Figure 2. Photograph of a 2-m-tall hornito erupted from a lava tube skylight ~1.9 km away from the primary vent. Hornitos erupt due to pressure built up from the release of magmatic water exsolution in very full lava tubes during the transport and are a type of secondary cone.

sediment-filled depression or coastline). Rootless cones are assumed when a more *clustered* geometry of features is observed and no obvious flows are seen emanating from the spatter features (Bruno et al., 2004). On Earth, hornitos are usually smaller than primary vents, have no significant lava flowing from them, and are situated along lava tubes instead of in clusters. Distal fissures are spatter outcrops exposed some distance away from the primary vent and are identified by their lack of lava flows and positive topography (cone or rampart). Rootless volcanic features have been hypothesized on Mars as evidence of water-lava interaction (Fagents et al., 2002; Fagents & Thordarson, 2007; Lanagan et al., 2001). More detailed imagery (e.g., rover cam) of the features on the Cerberus plains, Marte Valles, and Amazonis Planitia may allow for clast morphological analysis, which could allow researchers to determine the proportion of spatter and scoria in the deposits and examine the eruptive conditions of those features. To characterize the clast variability associated with a dry eruptive environment, we have analyzed spatter deposits at Craters of the Moon National Monument and Preserve.

Distinguishing between types of spatter even though broad contextual information has been lost to erosion or other factors would allow for the wider use of old spatter deposits for evaluating the thermal conditions of an eruption, potentially including the presence of water during emplacement. One study by Jones et al. (2018) has focused on the change in vesicle number density to distinguish between primary and secondary spatter environments. Our study classifies the variability within spatter deposits through clast size and shape, fusion between clasts, and void space within the deposit. Expanding this data set to include spatter deposits from rootless eruptions could allow our methods to be applied to rootless cone fields, complementing the work of Jones et al. (2018) and others (Fagents et al., 2002; Fagents & Thordarson, 2007; Lanagan et al., 2001).

2. Methods

2.1. Spatter Locations

Craters of the Moon National Monument and Preserve is a lava flow field located in Southern Idaho, USA (Figure 3). The volcanic system erupted ~30 km^3 of lava flows and pyroclasts from 15,000 to 2,000 years ago (Kuntz, Spiker, et al., 1986). The erupted material is predominantly mafic but SiO_2 can range from 44

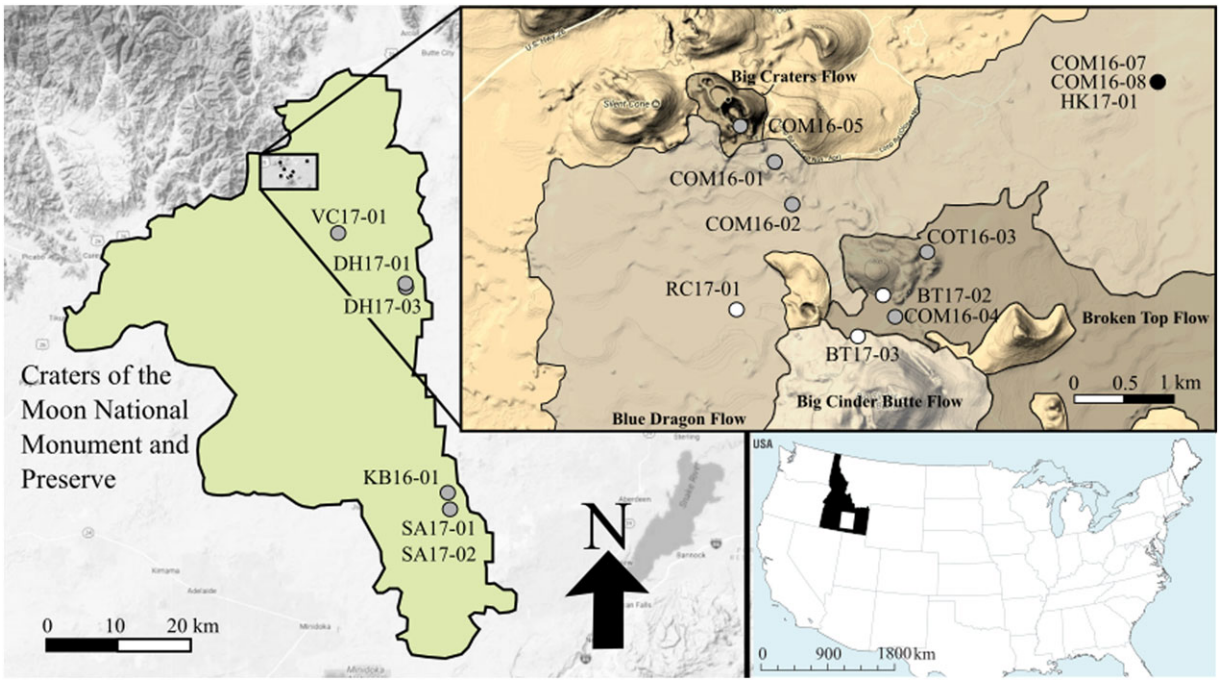

Figure 3. Map of sampled locations in Craters of the Moon National Monument and Preserve.

to 65% (Hughes et al., 1999; Kuntz et al., 1985). Flow units (e.g., Blue Dragon, Broken Top) with sampled spatter are some of the youngest in the Southern Idaho, between 6,600 and 2,000 years old, and have SiO_2 values between 44 and 57 wt. % (Table 1). Due to the relatively dry climate of Idaho, which limits the rates of postemplacement alteration and weathering, deposits are still quite fresh and glassy, leaving clast and deposit morphologies and textures well preserved (Davis, 1995).

In total, we investigated 16 outcrops with spatter deposits at Craters of the Moon National Monument and Preserve, Idaho (Figure 3, Table 1, and supporting information Table S5; Hughes et al, 2018; Kuntz et al, 1992, 2007). These sites were selected to represent an array of ages and chemical compositions while avoiding sensitive areas of the park. Eleven of these localities are in the northern portion of the monument, as access is easier and there are spatter features from numerous different flow units in relatively close proximity to one another. The four youngest eruptive periods in the region (ranging from ~2,000 to ~6,600 years old) all produced primarily basalt flows consisting of ʻaʻā, pāhoehoe, and transitional surface morphologies (Kuntz, Champion¸ et al., 1986). Sample sites that include spatter deposits in the Eruptive Period A (the youngest group in the Craters of the Moon region) were chosen from the Blue Dragon, Broken Top, Kings Bowl, and Big Craters lava flows (Figure 3). The next oldest eruptive period (B) includes spatter locations from Deadhorse and Vermillion Chasm flows. Older eruptive periods may be represented by spatter from Big Cinder Northwest (C), and Silent Cone (D); however, these two sites are isolated blocks that have been rafted from their original emplacement positions; they are not connected to any vent and are surrounded by younger lava. These two sites were deemed valuable despite their uncertain origin, because they illustrate how blocks of spatter may be found rafted or dislodged by an impact on planetary surfaces.

2.2. Outcrop Selection and Deposit Measurements

Outcrops were selected on the basis of near-vertical ~0.5-m^2 exposure and representativeness of the deposit. Regions of the outcrop that were highly deformed and fused, entering the clastogenic flow regime, were avoided; instead, we targeted deposits near the surface which experienced little loading from clasts above. The outcrop was photographed at several scales to allow for image analysis and documentation of the position of each clast. Contextual scale of the outcrop was captured in images taken ~5–10 m away to illustrate the relative position of the outcrop in the height of sampled feature. The outcrops are photographed from ~1 to 2 m away containing a scale to show the relative positions of the clasts and the space between the clasts.

Table 1
Morphological Measurements of Spatter Clasts

Sample name	Type	Flow unit	SiO_2	MgO	*n*	*F* value	Void space	Long axis	Short axis	*w/l*	Rind thickness	Rind vesicle size	Rind vesicle mode	Core vesicle size	Core vesicle mode	Hollow core
			(wt. %)	(wt. %)		(%)	(%)	(cm)	(cm)		(mm)	(mm)	(%)	(mm)	(%)	(%)
BT17–02	distal crack	Broken Top	49.47	3.36	75	6	0.6	3.9	1.7	0.93	1.6	0.5	20	3.1	52	0
BT17–03	distal crack	Big Cinder	54.91	2.17	109	4	8	3.1	2.4	0.97	2.6	0.8	16	5.4	54	0
RC17–01	distal crack	Silent Cone	55.84	1.59	137	3	2	2.0	1.5	0.97	5.0	1.0	29	2.8	50	0
COM16–07	hornito	Blue Dragon	49.06	3.35	12	22	10	23.0	8.0	0.47	2.3	0.7	13	6.1	67	17
COM16–08	hornito	Blue Dragon	49.06	3.35	11	15	6	26.0	8.6	0.45	1.5	0.7	10	7.5	65	27
HK17–01	hornito	Blue Dragon	49.06	3.35	18	14	9	15.8	7.3	0.49	3.6	1.0	24	5.3	54	0
COM16–01	primary vent	Blue Dragon	49.06	3.35	12	38	12	41.3	9.3	0.37	5.9	0.6	25	14.6	61	58
COM16–02	primary vent	Blue Dragon	49.06	3.35	18	18	15	29.0	8.0	0.35	5.9	0.5	20	11.9	64	6
COM16–03	primary vent	Broken Top	49.47	3.36	10	32	15	10.4	2.9	0.49	1.0	0.6	13	3.1	49	0
COM16–05	primary vent	Big Craters	51.02	2.86	16	42	14	17.6	6.0	0.41	1.6	0.6	20	4.7	57	12
DH17–01	primary vent	Deadhorse	45.15	6.33	12	49	8	25.9	6.0	0.33	1.4	0.3	9	2.5	51	17
DH17–03	primary vent	Deadhorse	45.15	6.33	11	38	7	23.5	6.5	0.40	2.5	1.4	14	3.5	49	0
KB16–01	primary vent	Kings Bowl	45.57	9.14	13	36	15	25.5	4.4	0.25	1.8	0.6	18	8.4	53	0
SA17–01	primary vent	Kings Bowl	45.57	9.14	15	29	10	25.2	7.7	0.36	1.1	0.3	6	3.0	50	53
SA17–02	primary vent	Kings Bowl	45.57	9.14	15	82	4	52.5	7.6	0.20	7.0	0.6	24	4.7	60	93
VC17–01	primary vent	Vermillion	45.84	5.99	17	33	21	14.8	5.6	0.42	3.1	0.6	15	4.8	51	0

Note. Values are the average of *n* clasts. Standard deviations are reported in the supporting information. SiO2 and MgO are averages for the flow unit published in Kuntz et al. (1985).

Up-close images were taken ~30–50 cm away with the intent of showing the details of vesiculation, rim thickness, and regions where clasts were fused together. All images were 72 and 300 ppi. Subsequently, the dimensions of the spatter deposit were measured and the void space between clasts was measured with the image processing software, Image J©, (Figure 4). Clasts were outlined and filled polygons were placed over void spaces between the clasts. The area of the void spaces was then calculated by comparing the number of pixels to the in-photo scale. All other measurements were done in the field.

2.3. Individual Clast Measurements

Within the cross section of an outcrop, a minimum of 10 clasts were outlined by following the glassy rind encircling the more vesicular core exposed along a vertical plane. Scoria clasts were determined by having a fractured outline with no glassy rim. A hammer and chisel were used to expose the cores of spatter clasts that were not already broken open. The morphological features of each measured spatter clast included vesicle size and mode, which were estimated by eye in both the rind and core of a clast (Figure 5). It was also noted if a hollow core was present or absent for each clast. If the core was hollow, then core vesicularity was determined by the mode of vesicles in the 2 cm surrounding the hollow core. The rind thickness and clast thickness (short axis) and length (long axis) were measured, as well as the clast perimeter. The

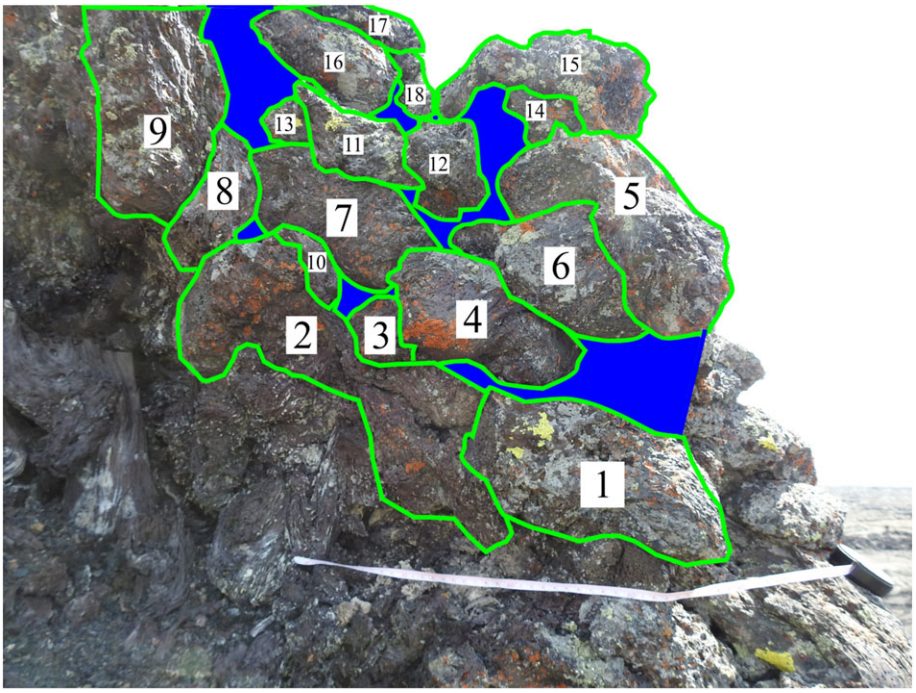

Figure 4. A photograph of HK17-01 showing the outlined, numbered clasts in green and void space between the clasts in blue. Cores of clasts that were not exposed were gently chiseled open so researchers could investigate the interior structure of each clast.

method of quantifying fusion between clasts was modified from Rader & Geist, 2015. We consider the average percentage of the perimeter fused to adjacent clasts is a proxy for thermal conditions and it is referred to as *F*.

$$F = 100 \times \frac{1}{n} \sum_{0}^{n} \left(\frac{\text{fused length}_{clast\ n}}{\text{perimeter}_{clast\ n}} \right)$$

A high *F* value implies a high heat flux either from high accumulation rate and/or high initial temperature. The absence or presence of a hollow core (Figure 5) was noted for each clast, with the percentage of hollow clasts in each deposit reported in Table 1.

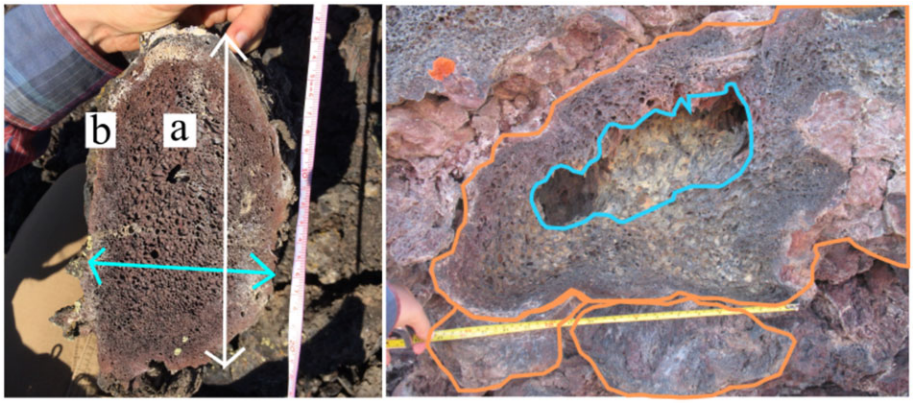

Figure 5. The photo on the left of an excavated clast shows some of the measurements collected, such as the long axis (white arrow), short axis (blue arrow) used to calculate clast aspect ratio, the mode of vesicles in the core (a) and in the quenched rim (b). The photo on the right of in situ clasts (outlined in orange) illustrates the hollow core (outlined in blue) that is often present in primary vent locations.

2.4. Sources of Error in Measurements

Measuring and estimating involves some error, particularly for interpretations of which clast contacts are fused as opposed to merely touching or estimating the mode of vesicles. Careful attention was paid to where clasts were in contact, with fusion being signaled by a distinct lack of a crack or clear boundary between clasts on a submillimeter scale. Whether clasts were fused or simply touching became more difficult to distinguish when there were high levels of alteration or lichen, and it was sometimes necessary to break clasts apart to better evaluate the strength of the connection. All the clasts in this study were measured by the same researcher to ensure consistency, and several clasts were remeasured to test the reproducibility of this method. *F* value measurements repeated on two clasts at COM16-05 were within 5% of each other, as were modal vesicularities, the most subjective of the field measurements.

For interclast void space, which is measured at each outcrop via digital images, each clast that intersected the exposed vertical plane was outlined and the area between clasts was measured by Image J©. Reproducibility was estimated by outlining spatter clasts on a photograph numerous times and calculating the difference between the trials. This was found to be generally less than 5%, and so this value is used as error bars on diagrams. A clast was deemed to have a hollow core if the size of the vesicles within 2 cm of the central void was 3X smaller than the central void itself. For these clasts, core vesicularity measurements were made in the 2 cm surrounding the hollow core.

3. Results

3.1. Characteristics That Correlate With Higher *F* Value

We compared morphological features with *F* value (shown to be a thermal proxy) for all spatter locations to identify which features were indicative of higher temperature, and/or faster accumulation rate (Figure 6). Correlation coefficients (*r* values) show the strength and direction of the correlation for each data set. As *F* increases, clast aspect ratio decreases (*r* of −0.68), while clast length (*r* of 0.63) and hollow core percent increase (*r* = 0.64). The percentage of between-clast void space in an outcrop generally decreases with increasing *F* when hornito and distal samples are excluded (*r* = −0.56; Figure 6). Any correlation between *F* and rind thickness, clast short axis, or vesicle measurements were not found to be distinguishing between primary and secondary spatter populations, and so *r* values are not reported for these characteristics.

3.2. Morphological Groupings of Eruptive Environment

3.2.1. Primary Vent

These types of spatter deposits are found proximal to the eruptive feature, be it a cone or a fissure. In our study, we used a narrow range limit of ~3 m from the source, both in order to ensure consistency and to reflect typical zones of spatter access in our field area. Spatter deposits at 10 localities, including deposits in the Blue Dragon, Broken Top, Big Craters, Vermillion Chasm, Deadhorse, and Kings Bowl units, typically exhibit higher *F* and lower aspect ratios than hornito or distal fissure spatter deposits (Figure 6). Overall variability within this category was very high in all measurements, including *F* values (18–82%), proportion of clasts containing hollow cores (0–93%), core vesicle mode (43–83%), aspect ratios (0.20–0.49), and void space (4–21%).

3.2.2. Hornito

All three hornito outcrops measured in this study are on a single cone on the eastern edge of the cave area in the Blue Dragon Flow. The spatter cone is located above a lava tube. The three locations were very consistent with one another, likely a function of their shared depositional history. *F* values for the hornito range from 14 to 22%, and have narrow ranges in the other measurements including void space (6–10%), aspect ratio (0.45–0.49), core vesicle mode (54–67%), and proportion of hollow cores (0–27%). Several other hornitos were located in the study area; however, they were very small and the researchers did not want to cause damage to these unique features and so the clasts were not measured.

3.2.3. Distal Fissure

Access to vertical sections of spatter distal from vents was found along noneruptive cracks in spatter deposit features at Deadhorse and Broken Top flows, and on rafted cone sections such as Silent Cone and Big Cinder NW flows (the underlying units in each outcrop location). These samples have a higher proportion of scoria clasts of uniform size which have no quench rind and no discernible gradient in vesicle size, or mode from rim to core than primary or hornito deposits. For these reasons, the only measurements made on scoria clasts

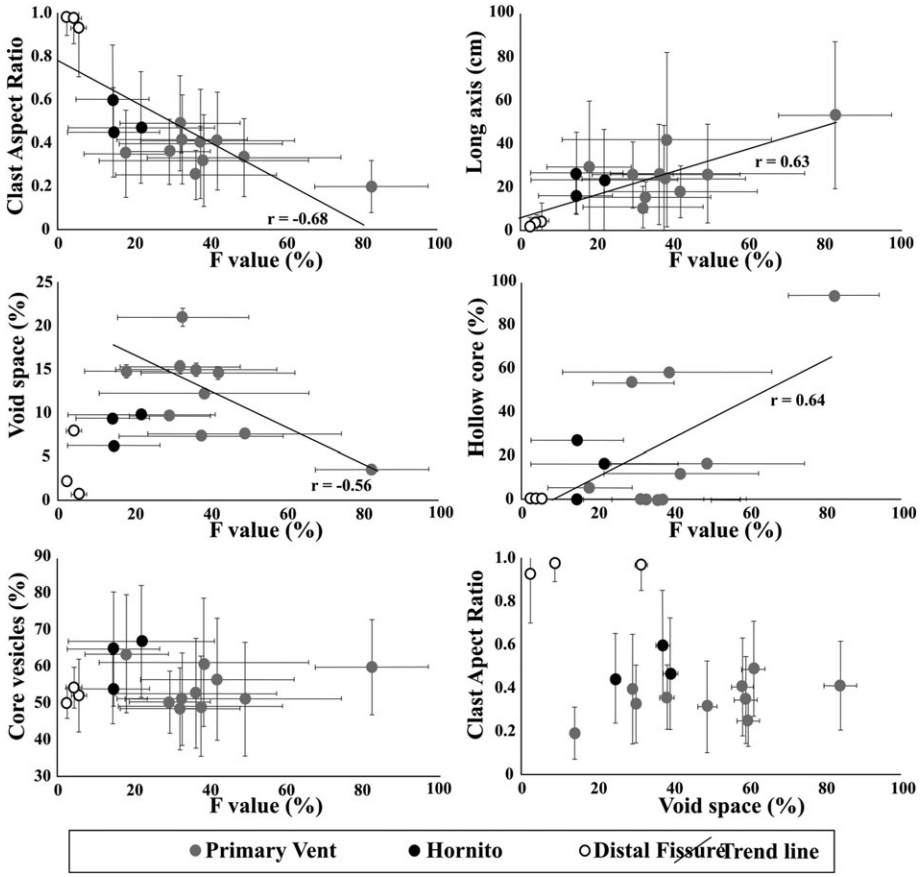

Figure 6. Graphs showing the relationship between measured features on spatter bombs. *F* value is used as a thermal proxy, with temperature increasing with higher *F*. Clast aspect ratio versus percent interclast void space appears to distinguish between primary vent, distal outcrops, and hornitos. As these are fairly easy measurements to make from a digital image, or using high-resolution LIDAR, this method could be used to distinguish between primary spatter or secondarily erupted spatter (from the presence of external gas) on other planetary bodies. Error bars show the variability in each outcrop for aspect ratio of clasts and are set at 5% for void space measurements (see section 4.1 for more discussion). White circles are distal fissures, black circles are hornito samples, and gray circles are primary vent localities.

were long and short axes. The value for each outcrop is an average of all the scoria clasts which have an *F* of 0%, and the measurements of the few spatter clasts. At the three measured outcrops, average values for clasts were similar such as average long axis (2–3.9 cm), aspect ratios (0.93–0.97) void space between clasts (0.6–8%), *F* value (3–6%), and were never hollow. Distal outcrops also contain more secondary alteration, primarily concentrated in the scoria-rich regions, which typically have higher porosity than spatter clasts due to the lack of dense glassy rims.

4. Discussion

4.1. Morphological Variability Within Outcrops

Natural eruptions will produce clasts of varying size and gas content which are transported higher or faster depending on where in the jet they are located and if they collide with any other particles during flight (e.g., Head & Wilson, 1986; Stovall et al., 2012; Vanderkluysen et al., 2012). Additionally, studies of fountaining basaltic systems show that emplacement temperatures for individual clasts can vary by hundreds of degrees, as clasts may be fresh or formed from ripped-up cooler crust or recycled fountain material (Carling et al., 2015; Davies et al., 2011; Mangan et al., 1995; Wilson et al., 1995). This leads to a wide variety of clasts morphologies within a single outcrop, necessitating a metric that captures the essence of the deposit as well as variability. For the sake of simplicity, we assume that the average and standard deviation (supporting information) of clast measurements associated with an outcrop offer a good representation of the general eruptive and

magmatic conditions for the eruption that formed that deposit, even though our data are not always normally distributed. As individual outcrops have limited numbers of clasts measured (*n* of 10–18), we discourage broad environmental interpretations based solely on these outcrops. Instead, we offer comparisons between the major categories of spatter (primary vent, hornito, and distal; clast $n > 41$ for each category).

4.2. Morphological Signs of Thermal History in Spatter Deposits

Several morphological features in spatter deposits correlate with the percentage of connections (*F* value) between clasts, a characteristic that has been experimentally linked to the temperature of the deposits including the number and strength of connections between spatter clasts (Rader & Geist, 2015). Vesicles can migrate and coalesce more easily in a hotter, less viscous lava, resulting in large hollow cores at higher temperatures if the lava was not degassed and there was gas exsolving from within the clast to begin with. Vesicle size distribution analysis of lava collected near the Pu'u' O'o vent and several kilometers down the flank show vesicle size and number decreasing away from the vent (Cashman et al., 1994), consistent with our measurements of more hollow cores in primary vent deposits than in hornito spatter deposits. However, we did not see significant changes in vesiculation (size or mode) in the core or rim of clasts with increasing *F*. This may be due to the lower resolution method of estimating modes compared to vesicle size distribution, the technique used by Jones et al. (2018), in which they saw higher vesicularity in primary spatter compared to secondary spatter. We chose the modal assessment of vesicularlity to avoid sampling and to allow our method to be applicable with remote sensing techniques. Despite not resolving vesicularity differences, measuring the proportion of clasts with a hollow core does signal a higher ($>$0.40) or lower ($<$0.40) emplacement temperature.

At higher temperatures, clasts deform into more elongate shapes, as seen by the aspect ratio and average clast length values. This deformation can occur during flight (stretching from the force of explosion), upon landing (gravitational impact), or after deposition as gas escapes and contracts during cooling. It can also occur from compaction if new clasts are exerting a significant weight from above (loading), but we do not consider this in our analyses as we chose outcrops to minimize this additional variable at this time. A previous analysis of clast shape in a primary vent spatter feature in North Iceland showed a similar relationship, with flatter clasts correlating positively with lower deposit void space and larger clast size (Reynolds et al., 2016). The aspect ratios (0.1–0.5) of the scoria cone spatter described in Reynolds et al. (2016) are similar to the primary vent spatter in this study (0.20–0.49) and exhibit similar variability.

This same tendency for clasts to deform more easily at higher temperatures explains the lower percentage of void spaces we see in the primary vent samples with a higher *F* value (Figure 6). Distal outcrops, being predominantly composed of small clasts, fill void space with solid clasts instead of drooping fluid clasts and have little space within a deposit despite low *F* values. Hornito samples also have lower void space than primary vents of equal *F* value, which may suggest that clasts may be able to deform and fill gaps at slightly lower temperatures than what is necessary for fusion between clasts.

4.3. Distinguishing Primary Vent Spatter, Distal Deposits, and Hornito Spatter

Primary vent eruptions are capable of producing the hottest and most gas-rich spatter deposits when lava is ejected quickly and has a short flight path. Recycling, ponding, long flight-times, or flowing of lava before it erupts at secondary cones will result in cooling, loss of gas, and stiffening of clasts. Hornitos, having erupted from lava that has been transported, degassed, and in a cooler environment relative to the vent, exhibit less welding between clasts, less flattening of clasts, and lower proportion of gas cavities in the core of clasts. The three hornito samples in this study seem to display lower temperature emplacement conditions; however, since there was only one hornito sampled, this trend is not statistically significant. Further study of additional hornitos as well as predominantly scoria rootless cones would allow for a more quantitative distinction between primary vents and rootless features. With more study, it is possible that comparing aspect ratios of clasts and void space within deposits will show the greatest difference between eruption environments (Figure 6).

The differences in spatter between hornitos, primary vents, and distal fissures suggest the possibility of developing spatter observation and measurement metrics that could differentiate between eruptive conditions. Our methods would complement the statistical analyses of rootless cone field distribution studies (Bruno et al., 2004, 2006) and help interpret thermal conditions for stratigraphic analyses of rootless cones such as

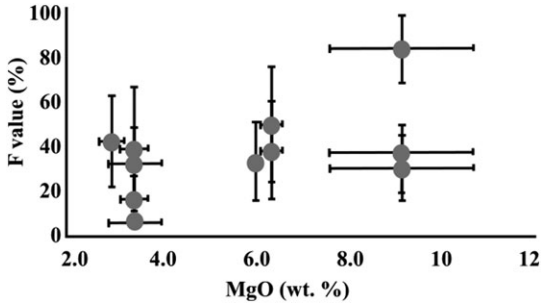

Figure 7. Whole-rock MgO wt. % analyses from the same flow units as the spatter collected in this study plotted against the percent connectedness of the clasts within primary vent outcrops. Analyses are from Kuntz et al. (1985) and show a mild trend of higher-temperature lava (higher MgO wt. %) resulting in more connectedness between clasts. This suggests that chemical composition has an effect on the eruption temperature, but the variability within each grouping of MgO wt. % illustrates how other factors, such as recycling or flight time of clasts, as well as accumulation rate, can be at play.

Hamilton et al., 2017 and Reynolds et al., 2016. This could be particularly useful in the evaluation of disjoined spatter-bearing outcrops where contextual information is not available, such as in ejecta blocks around craters on planetary surfaces. However, this data set needs to be expanded to include spatter measurements on rootless cone fields that conclusively interacted with water or ice to be applicable to environmental conditions.

4.4. Causes of Fusion in Spatter Clasts

Previous studies that examine spatter clast morphology (e.g., Reynolds et al., 2016; Sánchez et al., 2012) attribute changes in deposit morphology (clast morphology and deposit void space) to the change in accumulation rate, with more densely welded spatter representing higher accumulation rates. These studies assumed that the temperature of the clasts did not change substantially over the course of the eruption due to the lack of chemical variation in the lava during the eruption.

Eruption temperatures can be related to the chemical composition of lava if the magma thermally equilibrated shortly before eruption (e.g., Ghiorso & Sack, 1991; Helz & Thornber, 1987; Loucks, 1996). Generally, in low-silica melts that are in equilibrium with olivine, magmas with lower MgO wt. % will erupt at lower temperatures. Most of the Craters of the Moon National Monument and Preserve rocks contain euhedral olivine, as reported by Kuntz, Champion¸ et al. (1986) and Stout et al. (1994). Primary vent *F* values were plotted against MgO wt. % data published by Kuntz et al. (1985) and shows a correlation with fusion and chemical evolution (Figure 7). The spatter deposits cluster into three groups, highest eruption temperature (MgO $>$ 9 wt. %, high *F*), moderate eruption temperature (5.5–6.5 wt. % MgO, moderate *F*), and lowest eruption temperature (MgO $<$ 4 wt.%, low *F*). This suggests that more evolved magmas (lower MgO) erupted spatter at lower initial temperatures than magmas with less SiO_2 and more MgO. The present study does not include enough samples to resolve any differences in the data due to differing chemical composition. If the majority of material that erupted during a single event is of a similar chemical composition, then the variability of fusion within a unit may be due predominantly to accumulation rate. Additional research emphasizing within-unit spatter deposits is required to test this hypothesis.

4.5. Viability of Method for Planetary Geology

Measuring spatter clasts has shown promise for distinguishing types of spatter deposits and deducing relative rates of cooling, such as by distinguishing hornitos from primary vent spatter. With some modification this method could be used to analyze images of potential spatter deposits on the Moon and Mars. Some measurements are more conducive to collection by remote sensing, such as clast aspect ratio, void space between clasts, and hollow cores, so these should be preferentially used. Additionally, some calibration for different atmospheric and gravity effects would need to be taken into consideration. Studies of vesicle size on Earth have shown that small changes in pressure due to elevation of lava emplacement can have an effect on vesicle size (Sahagian & Maus, 1994; Sahagian & Proussevitch, 2007), and the difference in vesicle size between the top and bottom of lava flows has been used to calculate lower atmospheric pressure of Early Earth (Som et al., 2016), suggesting that vesicle sizes in spatter may be reflective of the Mars atmospheric pressure since proximity to the vent does not appear to affect vesicle size other than the coalescence of gas into a hollow core.

It may also be possible to categorize the degrees of welding based on visual inspection of the image, as opposed to measuring the proportion of connections that are fused together, which typically has to be done in situ. This type of analysis would greatly benefit from high-resolution imagery taken by robotic lander or rover, which would allow researchers to zoom in on clast contacts. Software-assisted tracing could automate the process as well, leading to large data sets that could improve the statistical significance of measurements.

5. Conclusion

The shape, size, and vesicularity of spatter clasts, along with the between-clast void space in a deposit, are affected by the overall temperature during emplacement. In general, higher temperatures cause clasts

with similar chemical compositions, crystal content, and gas content to have lower viscosities, resulting in great mobility of gas within the clast and more fluid deformation of the clast itself. In general, spatter deposits with few hollow cores, larger void spaces, more rounded and smaller clasts will have formed at lower emplacement temperatures than deposits with numerous hollow cores, fewer void spaces, and larger, oblate clast shapes. It is challenging to estimate accumulation rate between spatter locations because numerous additional thermal factors, such as varying chemical composition, fountain height, or degree of recycling may vary at any point in time. Without further study characterizing the frequency in these factors changing in actual eruptions, relative accumulation rates should only be estimated within a single feature, such as a small cone or rampart. This study did not sample sufficient clasts populations to statistically distinguish between accumulation rates at different features. Due to the strong effect of temperature on clast morphology, spatter deposits that form very near a vent are distinguishable from distal deposits and less so, hornito deposits. This is most easily seen when comparing average clast aspect ratios to the void space. Identifying the eruption condition (primary vent or secondary vent) has implications for the categorization of inaccessible pyroclastic deposits through digital image analysis, which may be applied to nonterrestrial outcrops once the empirical relationship between clast morphology and depositional environment is calibrated for gravitational and thermal conditions, including the presence of water.

Acknowledgments
This research was supported by the NASA Postdoctoral Program (administered by USRA) and FINESSE (Field Investigation to Enable Solar System Science and Exploration, PI J.L. Heldmann), a SSERVI research grant to NASA Ames Research Center. Field work was conducted under NPS permit CRMO-2014-SCI-0004. We thank Craters of the Moon National Monument and Preserve and the people of Arco, Idaho, for their support during the project. Field support was provided by FINESSE team members and Cara Stoddard. The authors greatly appreciate comments by Alex Sehlke, Derek Sears, and Scott Hughes, to improve the manuscript. Data for this manuscript are available in the supporting information and in included tables.

References

Brown, R. J., Blake, S., Thordarson, T., & Self, S. (2014). Pyroclastic edifices record vigorous lava fountains during the emplacement of a flood basalt flow field, Roza Member, Columbia River Basalt Province, USA. *Geological Society of America Bulletin*, *126*(7–8), 875–891. https://doi.org/10.1130/B30857.1

Bruno, B. C., Fagents, S. A., Hamilton, C. W., Burr, D. M., & Baloga, S. M. (2006). Identification of volcanic rootless cones, ice mounds, and impact craters on Earth and Mars: Using spatial distribution as a remote sensing tool. *Journal of Geophysical Research*, *111*, E06017. https://doi.org/10.1029/2005JE002510

Bruno, B. C., Fagents, S. A., Thordarson, T., Baloga, S. M., & Pilger, E. (2004). Clustering within rootless cone groups on Iceland and Mars: Effect of nonrandom processes. *Journal of Geophysical Research*, *109*, E07009. https://doi.org/10.1029/2004JE002273

Capaccioni, B., & Cuccoli, F. (2005). Spatter and welded air fall deposits generated by fire-fountaining eruptions: Cooling of pyroclasts during transport and deposition. *Journal of Volcanology and Geothermal Research*, *145*(3-4), 263–280. https://doi.org/10.1016/j.jvolgeores.2005.02.001

Carling, G. T., Radebaugh, J., Saito, T., Lorenz, R. D., Dangerfield, A., Tingey, D. G., et al. (2015). Temperatures, thermal structure, and behavior of eruptions at Kilauea and Erta Ale volcanoes using a consumer digital camcorder. *GeoResJ*, *5*, 47–56. https://doi.org/10.1016/j.grj.2015.01.001

Cashman, K. V., Mangan, M. T., & Newman, S. (1994). Surface degassing and modifications to vesicle size distributions in active basalt flows. *Journal of Volcanology and Geothermal Research*, *61*(1–2), 45–68. https://doi.org/10.1016/0377-0273(94)00015-8

Davies, A. G., Keszthelyi, L., & McEwen, A. S. (2011). Estimating eruption temperature from thermal emission spectra of lava fountain activity in the Erta'Ale (Ethiopia) volcano lava lake: Implications for observing Io's volcanoes. *Geophysical Research Letters*, *38*, L21308. https://doi.org/10.1029/2011GL049418

Davis, O. K. (1995). Climate and vegetation patterns in surface samples from arid western USA: Application to Holocene climatic reconstructions. *Palynology*, *19*(1), 95–117. https://doi.org/10.1080/01916122.1995.9989454

Fagents, S. A., Lanagan, P., & Greeley, R. (2002). Rootless cones on Mars: A consequence of lava-ground ice interaction. *Geological Society, London, Special Publications*, *202*(1), 295–317. https://doi.org/10.1144/GSL.SP.2002.202.01.15

Fagents, S. A., & Thordarson, T. (2007). Rootless volcanic cones in Iceland and on Mars. In *The geology of Mars: Evidence from Earth-based analogs*, (pp. 151–177). Cambridge: Cambridge University Press. https://doi.org/10.1017/CBO9780511536014.007

Gao, W., Li, J., Mao, X., & Zhang, T. (2010, May). Genetic mechanism of hornitos in Wudalianchi Volcanic Field, Northeast China. *EGU General Assembly Conference Abstracts*, *12*, 6264.

Ghiorso, M. S., & Sack, O. (1991). Fe-Ti oxide geothermometry: Thermodynamic formulation and the estimation of intensive variables in silicic magmas. *Contributions to Mineralogy and Petrology*, *108*(4), 485–510. https://doi.org/10.1007/BF00303452

Hamilton, C. W., Fitch, E. P., Fagents, S. A., & Thordarson, T. (2017). Rootless tephra stratigraphy and emplacement processes. *Bulletin of Volcanology*, *79*(1), 11. https://doi.org/10.1007/s00445-016-1086-4

Hamilton, C. W., Thordarson, T., & Fagents, S. A. (2010). Explosive lava–water interactions I: Architecture and emplacement chronology of volcanic rootless cone groups in the 1783–1784 Laki lava flow, Iceland. *Bulletin of Volcanology*, *72*(4), 449–467. https://doi.org/10.1007/s00445-009-0330-6

Head, J. W., & Wilson, L. (1986). Volcanic processes and landforms on Venus: Theory, predictions, and observations. *Journal of Geophysical Research*, *91*, 9407–9446. https://doi.org/10.1029/JB091iB09p09407

Head, J. W. III, & Wilson, L. (1989). Basaltic pyroclastic eruptions: Influence of gas-release patterns and volume fluxes on fountain structure, and the formation of cinder cones, spatter cones, rootless flows, lava ponds and lava flows. *Journal of Volcanology and Geothermal Research*, *37*(3–4), 261–271. https://doi.org/10.1016/0377-0273(89)90083-8

Helz, R. T., & Thornber, C. R. (1987). Geothermometry of Kilauea Iki lava lake, Hawaii. *Bulletin of Volcanology*, *49*(5), 651–668. https://doi.org/10.1007/BF01080357

Hughes, S. S., Nawotniak, S. E. K., Sears, D. W., Borg, C., Garry, W. B., Christiansen, E. H., et al. (2018). Phreatic Explosions During Basaltic Fissure Eruptions: Kings Bowl Lava Field, Snake River Plain, USA. *Journal of Volcanology and Geothermal Research*, *351*, 89–104.

Hughes, S. S., Smith, R. P., Hackett, W. R., & Anderson, S. R. (1999). Mafic volcanism and environmental geology of the eastern Snake River Plain, Idaho. In *Guidebook to the geology of eastern Idaho*, (pp. 143–168). Pocatello, ID: Idaho Museum of Natural History.

Jones, T. J., Houghton, B. F., Llewellin, E. W., Parcheta, C. E., & Höltgen, L. (2018). Spatter matters–distinguishing primary (eruptive) and secondary (non-eruptive) spatter deposits. *Scientific Reports*, *8*(1), 9179. https://doi.org/10.1038/s41598-018-27065-1

Jurado-Chichay, Z., Rowland, S. K., & Walker, G. P. (1996). The formation of circular littoral cones from tube-fed pāhoehoe: Mauna Loa, Hawai'i. *Bulletin of Volcanology*, *57*(7), 471–482.

Kauahikaua, J., Sherrod, D. R., Cashman, K. V., & Heliker, C. (2003). Hawaiian lava-flow dynamics during the Pu 'u "O" o. *The Pu 'u 'O 'o–Kupaianaha eruption of Kilauea volcano, Hawai 'i: the first, 20*, 63–87.

Kuntz, M. A., Champion, D. E., Spiker, E. C., & Lefebvre, R. H. (1986). Contrasting magma types and steady-state, volume-predictable, basaltic volcanism along the great rift, Idaho. *Geological Society of America Bulletin*, *97*(5), 579–594. https://doi.org/10.1130/0016-7606(1986)97<579:CMTASV>2.0.CO;2

Kuntz, M. A., Covington, H. R., & Schorr, L. J. (1992). An overview of basaltic volcanism of the eastern Snake River plain, Idaho. *Regional geology of Eastern Idaho and Western Wyoming: Geological society of America memoir*, *179*, 227–267. https://doi.org/10.1130/MEM179-p227

Kuntz, M. A., Elsheimer, H. N., Espos, L. F., & Klock, P. R. (1985). Major-element analyses of latest Pleistocene-Holocene lava fields of the Snake River plain, Idaho (No. 85-593). US Geological Survey.

Kuntz, M. A., Skipp, Betty, Champion, D. E., Gans, P. B., Van Sistine, D. P., & Snyders, S. R. (2007). Geologic map of the craters of the Moon 30′ × 60′ quadrangle, Idaho: *U.S. Geological Survey Scientific Investigations Map* 2969, 64-p. pamphlet, 1 plate, scale 1:100,000.

Kuntz, M. A., Spiker, E. C., Rubin, M., Champion, D. E., & Lefebvre, R. H. (1986). Radiocarbon studies of latest Pleistocene and Holocene lava flows of the Snake River plain, Idaho: Data, lessons, interpretations. *Quaternary Research*, *25*(02), 163–176. https://doi.org/10.1016/0033-5894(86)90054-2

Lanagan, P. D., McEwen, A. S., Keszthelyi, L. P., & Thordarson, T. (2001). Rootless cones on Mars indicating the presence of shallow equatorial ground ice in recent times. *Geophysical Research Letters*, *28*, 2365–2367. https://doi.org/10.1029/2001GL012932

Loucks, R. R. (1996). A precise olivine-augite mg-Fe-exchange geothermometer. *Contributions to Mineralogy and Petrology*, *125*(2-3), 140–150. https://doi.org/10.1007/s004100050211

Mangan, M. T., Heliker, C. C., Mattox, T. N., Kauahikaua, J. P., & Helz, R. T. (1995). Episode 49 of the Pu'u'O'o-Kupaianaha eruption of Kilauea volcano-breakdown of a steady-state eruptive era. *Bulletin of Volcanology*, *57*(2), 127–135.

Mattox, T. N., & Mangan, M. T. (1997). Littoral hydrovolcanic explosions: A case study of lava–seawater interaction at Kilauea volcano. *Journal of Volcanology and Geothermal Research*, *75*(1–2), 1–17. https://doi.org/10.1016/S0377-0273(96)00048-0

Rader, E., & Geist, D. (2015). Eruption conditions of spatter deposits. *Journal of Volcanology and Geothermal Research*, *304*, 287–293. https://doi.org/10.1016/j.jvolgeores.2015.09.011

Reynolds, P., Brown, R. J., Thordarson, T., & Llewellin, E. W. (2016). The architecture and shallow conduits of Laki-type pyroclastic cones: Insights into a basaltic fissure eruption. *Bulletin of Volcanology*, *78*(5), 36. https://doi.org/10.1007/s00445-016-1029-0

Reynolds, P., Brown, R. J., Thordarson, T., Llewellin, E. W., & Fielding, K. (2015). Rootless cone eruption processes informed by dissected tephra deposits and conduits. *Bulletin of Volcanology*, *77*(9), 72. https://doi.org/10.1007/s00445-015-0958-3

Sahagian, D., & Proussevitch, A. (2007). Paleoelevation measurement on the basis of vesicular basalts. *Reviews in Mineralogy and Geochemistry*, *66*(1), 195–213. https://doi.org/10.2138/rmg.2007.66.8

Sahagian, D. L., & Maus, J. E. (1994). Basalt vesicularity as a measure of atmospheric pressure and palaeoelevation. *Nature*, *372*(6505), 449–451. https://doi.org/10.1038/372449a0

Sánchez, M. C., Sarrionandia, F., Arostegui, J., Eguiluz, L., & Ibarguchi, J. G. (2012). The transition of spatter to lava-like body in lava fountain deposits: Features and examples from the Cabezo Segura volcano (Calatrava, Spain). *Journal of Volcanology and Geothermal Research*, *227*, 1–14.

Shin, H., Lindquist, W. B., Sahagian, D. L., & Song, S. R. (2005). Analysis of the vesicular structure of basalts. *Computers & Geosciences*, *31*(4), 473–487. https://doi.org/10.1016/j.cageo.2004.10.013

Som, S. M., Buick, R., Hagadorn, J. W., Blake, T. S., Perreault, J. M., Harnmeijer, J. P., & et al. (2016). Earth's air pressure 2.7 billion years ago constrained to less than half of modern levels. *Nature Geoscience*, *9*(6), 448–451. https://doi.org/10.1038/ngeo2713

Stout, M. Z., Nicholls, J., & Kuntz, M. A. (1994). Petrological and mineralogical variations in 2500–2000 yr BP lava flows, craters of the moon lava field, Idaho. *Journal of Petrology*, *35*(6), 1681–1715. https://doi.org/10.1093/petrology/35.6.1681

Stovall, W. K., Houghton, B. F., Hammer, J. E., Fagents, S. A., & Swanson, D. A. (2012). Vesiculation of high fountaining Hawaiian eruptions: Episodes 15 and 16 of 1959 Kīlauea Iki. *Bulletin of Volcanology*, *74*(2), 441–455. https://doi.org/10.1007/s00445-011-0531-7

Sumner, J. M. (1998). Formation of clastogenic lava flows during fissure eruption and scoria cone collapse: The 1986 eruption of Izu-Oshima volcano, eastern Japan. *Bulletin of Volcanology*, *60*(3), 195–212. https://doi.org/10.1007/s004450050227

Sumner, J. M., Blake, S., Matela, R. J., & Wolff, J. A. (2005). Spatter. *Journal of Volcanology and Geothermal Research*, *142*(1-2), 49–65. https://doi.org/10.1016/j.jvolgeores.2004.10.013

Thordarson, T., & Hoskuldsson, A. (2002). Iceland. In *Classic geology in Europe, 3* (chap. 3, 200 pp.). Harpenden, UK: Terra Publishing.

Thordarson, T., Morrissey, M. M., Larsen, G., & Cyrusson, H. (1992). Origin of rootless cone complexes in S-Iceland. Abstract in the 20th Nordic geological winter meeting, ed. A. Geirsdo´ ttir, H. Norddahl, and G. Helgado´ ttir. Reykjavı'k: Icelandic Geoscience Society, p. 169.

Vanderkluysen, L., Harris, A. J., Kelfoun, K., Bonadonna, C., & Ripepe, M. (2012). Bombs behaving badly: Unexpected trajectories and cooling of volcanic projectiles. *Bulletin of Volcanology*, *74*(8), 1849–1858. https://doi.org/10.1007/s00445-012-0635-8

Wilson, L., Parfitt, E. A., & Head, J. W. (1995). Explosive volcanic eruptions—VIII. The role of magma recycling in controlling the behaviour of Hawaiian-style lava fountains. *Geophysical Journal International*, *121*(1), 215–225. https://doi.org/10.1111/j.1365-246X.1995.tb03522.x